Superconductivity in FeSe Thin Films Driven by the Interplay between Nematic Fluctuations and Spin-Orbit Coupling

Jian Kang* and Rafael M. Fernandes
School of Physics and Astronomy, University of Minnesota, Minneapolis, Minnesota 55455, USA
(Received 8 June 2016; published 18 November 2016)

The origin of the high-temperature superconducting state observed in FeSe thin films, whose phase diagram displays no sign of magnetic order, remains a hotly debated topic. Here we investigate whether fluctuations arising due to the proximity to a nematic phase, which is observed in the phase diagram of this material, can promote superconductivity. We find that nematic fluctuations alone promote a highly degenerate pairing state, in which both s-wave and d-wave symmetries are equally favored, and T_c is consequently suppressed. However, the presence of a sizable spin-orbit coupling or inversion symmetry breaking at the film interface lifts this harmful degeneracy and selects the s-wave state, in agreement with recent experimental proposals. The resulting gap function displays a weak anisotropy, which agrees with experiments in monolayer FeSe and intercalated $Li_{1-x}(OH)_xFeSe$.

DOI: 10.1103/PhysRevLett.117.217003

In most iron-based superconductors (FeSC), superconductivity is found in close proximity to a magnetically ordered state, suggesting that magnetic fluctuations play an important role in binding the Cooper pairs [1–4]. Indeed, the fact that the Fermi surface of these materials is composed of small hole pockets and electron pockets separated by the magnetic ordering vector led to the proposal of a sign-changing s^{+-} wave state, in which the gap function has different signs in the hole and in the electron pockets. However, the recent observation of superconductivity over 70 K in monolayer FeSe brought new challenges to the field [5–14]. In contrast to the standard FeSC, no long-range magnetic order is observed in thin films or even bulk FeSe [15], and the Fermi surface of monolayer FeSe consists of electron pockets only [6,7,11,16]. Since T_c in monolayer FeSe is the highest among all FeSC, the elucidation of its origin is a fundamental step in the search for higher T_c in these systems.

One of the proposed scenarios to explain the dramatic tenfold increase of T_c in monolayer FeSe with respect to the 8 K value in bulk FeSe [17] was the strong coupling to an optical phonon mode of the $SrTiO_3$ (STO) substrate [16,18,19], which is manifested by replica bands observed in ARPES [16]. Although such a coupling can certainly enhance T_c [20–24], recent experiments indicate that the STO substrate may not be essential to achieve the high-T_c state. In particular, T_c up to 40 K was observed in electrostatically gated films of FeSe with different thickness grown both on STO and MgO substrates [25]. Similar values of T_c were reported in FeSe coated with potassium [26,27] and in the bulk sample $Li_{1-x}(OH)_xFeSe$ [28,29], which consists of intercalated FeSe layers. In common to all these systems is the fact that their Fermi surface consists of electron pockets only, suggesting that doping by negative charge carriers plays a fundamental role in stabilizing the high-T_c state.

Importantly, recent experiments in K-coated bulk FeSe [26] revealed that, besides shifting the chemical potential, electron doping also suppresses the nematic order observed in undoped bulk FeSe at $T_{\rm nem} \approx 90$ K [30]. In the nematic state, whose origin remains hotly debated [31–35], the x and y in-plane directions become inequivalent and orbital order emerges. Remarkably, the highest T_c in the phase diagram of K-coated FeSe is observed near the region where $T_{\rm nem}$ nearly vanishes. Similarly, in the case of FeSe thin films grown on STO, nematic order is observed over a wide range of film thickness [36,37], but not in the monolayer case [38]. These observations, combined with the absence of magnetic order in these systems, begs the question of whether nematic fluctuations can provide a sensible mechanism to explain the superconductivity of thin films of FeSe [22,26,39,40].

In this Letter, we show that nematic fluctuations alone favor degenerate s-wave (A_{1g}) and d-wave (B_{2g}) superconducting states in FeSe thin films. This degeneracy stems from the fact that while the two electron pockets are separated by the momentum $\boldsymbol{Q}_M = (\pi, \pi)$, nematic fluctuations are peaked at $\boldsymbol{Q}_{\rm nem} = 0$. More importantly, the SC ground state manifold has an enlarged $U(1) \times U(1)$ degeneracy, which is very detrimental to SC, since fluctuations of one SC channel strongly suppress long-range order in the other SC channel. Remarkably, this degeneracy is removed by the sizable spin-orbit coupling (SOC) observed in these compounds [41], which lift the pairing frustration and selects s wave over d wave, stabilizing a SC state at higher temperatures. In thin films, the inversion symmetry breaking (ISB) at the interface also contributes significantly to this degeneracy lifting. Interestingly, recent experiments propose that an s-wave state is realized in FeSe

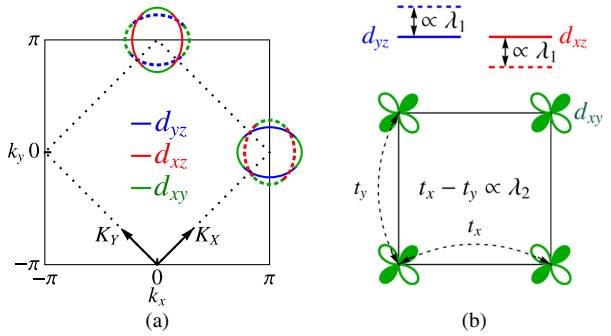

FIG. 1. (a) Fermi surface (FS) of a thin film of FeSe, consisting only of electron pockets, in the unfolded (solid lines) and folded (dotted lines) Brillouin zones. The color around the FS indicates the orbital that contributes to the largest spectral weight. (b) The two different nematic couplings: λ_1 couples to the on-site energy difference between the d_{xz} and d_{yz} orbitals, whereas λ_2 couples to the anisotropic hopping between nearest-neighbor d_{xy} orbitals.

thin films [42]. We also find that, when the SOC and/or ISB energy scales are larger than the energy scale associated with the mismatch between the two electron pockets, a nearly isotropic gap appears at the electron pockets, whose angular dependence agrees with ARPES and STM measurements in FeSe thin films [26,43] and intercalated $Li_{1-x}(OH)_xFeSe$ [44].

Microscopic model.—We start with the full five-orbital tight-binding model in the 1-Fe Brillouin zone and project it on the subspace of the d_{xz}, d_{yz}, and d_{xy} orbitals, which give the largest contribution to the Fermi surface. In particular, while the X electron pocket centered at $\boldsymbol{Q}_X = (\pi, 0)$ has d_{yz}/d_{xy} orbital content, the Y electron pocket centered at $\boldsymbol{Q}_Y = (0, \pi)$ has d_{xz}/d_{xy} content [see Fig. 1(a)]. Following Ref. [45], we expand the projected tight-binding matrix in powers of the momentum measured relative to $\boldsymbol{Q}_X$ and $\boldsymbol{Q}_Y$. Defining two spinors corresponding to each electron pocket,

$$\begin{aligned} \Psi_X(\boldsymbol{k}) &\approx (d_{yz}(\boldsymbol{k}+\boldsymbol{Q}_X), \quad d_{xy}(\boldsymbol{k}+\boldsymbol{Q}_X))^T, \\ \Psi_Y(\boldsymbol{k}) &\approx (d_{xz}(\boldsymbol{k}+\boldsymbol{Q}_Y), \quad d_{xy}(\boldsymbol{k}+\boldsymbol{Q}_Y))^T, \end{aligned} \tag{1}$$

the noninteracting Hamiltonian is written as $\mathcal{H}_0 = \sum_{\boldsymbol{k},i=X,Y} \Psi_i^\dagger(\boldsymbol{k}) \hat{H}_i(\boldsymbol{k}) \Psi_i(\boldsymbol{k})$, where $\hat{H}_i$ are 2×2 matrices in spinor space (see the Supplemental Material [46]). The B_{2g} nematic order parameter is described by the bosonic field ϕ_q, with $q = (\Omega_n, \boldsymbol{q})$, whereas the nematic fluctuations are given by the nematic susceptibility $\chi_{\rm nem}(\boldsymbol{q}, \Omega_n)$. For our analysis, it is not necessary to specify the origin of the nematic order parameter, but rather how it couples to the electronic states. As discussed in Ref. [48], there are two possible nematic couplings: λ_1, which couples ϕ_q to the on site energy difference between the d_{xz} and d_{yz} orbitals, and λ_2, which couples ϕ_q to the hopping anisotropy between nearest-neighbor d_{xy} orbitals [see Fig. 1(b)]:

$$\mathcal{H}_{\rm int} = \sum_{\boldsymbol{q},i=X,Y} \phi_{-\mathbf{q}} \Psi_i^\dagger(\boldsymbol{k}) \hat{\lambda}_i^{\rm nem} \Psi_i(\boldsymbol{k}+\boldsymbol{q}), \tag{2}$$

with $\hat{\lambda}_i^{\rm nem} = \pm {\rm diag}(\lambda_1, \lambda_2)$, where the plus (minus) sign refers to $i = X$ ($i = Y$). Here, we focus on the effect of short-ranged frequency independent nematic fluctuations and approximate $\chi_{\rm nem}(\boldsymbol{q}, \Omega_n)$ by its zero momentum and zero frequency value. The first approximation is justified due to the smallness of the electron pockets, whereas the second one is reasonable as long as the system is not too close to a nematic quantum critical point [40,49,50]. Note that renormalization-group calculations on a related microscopic model support the idea that the disappearance of the central hole pockets suppresses nematic order [32].

Superconducting instability.— We decompose the pairing states in terms of the different irreducible representations of the space group of the FeSe plane, $P4/nmm$ (see Ref. [45] and the Supplemental Material [46]), and focus on the two leading pairing channels, which belong to the singlet s-wave (A_{1g}) and d-wave (B_{2g}) symmetry representations [51]:

$$\Psi_X^T \begin{pmatrix} \Delta_1 & 0 \\ 0 & \Delta_2 \end{pmatrix} \otimes i\sigma_2 \Psi_X \pm \Psi_Y^T \begin{pmatrix} \Delta_1 & 0 \\ 0 & \Delta_2 \end{pmatrix} \otimes i\sigma_2 \Psi_Y, \tag{3}$$

where the plus (minus) sign refers to s-wave (d-wave) pairing. The gaps Δ_1 and Δ_2 correspond to intraorbital pairing within the d_{xz}/d_{yz} orbitals and d_{xy} orbitals, respectively. Δ_1 and Δ_2 are found via the gap equations

$$\eta \hat{M} = \chi_{\rm nem} T \sum_{n,\boldsymbol{k}} (\hat{\lambda}_i^{\rm nem})^T \hat{G}_{-k,i}^T \hat{M} \hat{G}_{k,i} \hat{\lambda}_i^{\rm nem}, \tag{4}$$

where η is the SC eigenvalue, $\hat{M} = \begin{pmatrix} \Delta_1 & 0 \\ 0 & \Delta_2 \end{pmatrix}$, and $\hat{G}_{p,i}^{-1} = i\omega_n - \hat{H}_i(\mathbf{p})$. The SC transition temperature is obtained when $\eta = 1$. Hereafter, we set the value of $(\lambda_1^2 + \lambda_2^2)\chi_{\rm nem}$ to yield $T_c = 5$ meV when $\lambda_2 = 0$.

Solution of the gap equations reveals that for all ratios of the nematic coupling constants λ_1 and λ_2, the superconducting instabilities in the s-wave and d-wave channels are always degenerate, as shown in Fig. 2(a). Although the intraorbital gaps Δ_1 and Δ_2 are isotropic, the gaps projected onto the Fermi pockets, Δ_X and Δ_Y, acquire an angle dependence due to the orbital content of the Fermi pockets. To illustrate this behavior, Fig. 2(b) shows Δ_X as a function of the polar angle θ. When $\lambda_1 > \lambda_2$, nematic fluctuations couple mainly to the d_{xz}/d_{yz} orbitals; as a result, Δ_X is proportional to the spectral weight of the d_{xz}/d_{yz} orbital on the X pockets, which is maximum around $\theta = \pm\pi/2$ [see Fig. 1(a)]. Consequently, Δ_X reaches its maximum at $\theta = \pm\pi/2$ and its minimum at $\theta = 0, \pi$. Conversely, for $\lambda_1 < \lambda_2$, the gap is maximum at $\theta = 0, \pi$, where the spectral

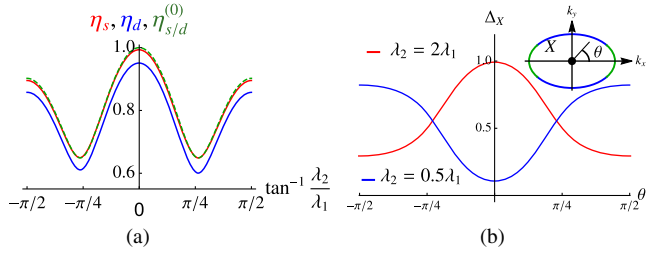

FIG. 2. (a) The eigenvalue η of the gap equation (4) as a function of the ratio between the two nematic couplings λ_2/λ_1. Without SOC or ISB, the s-wave and d-wave solutions have the same eigenvalue (dashed green curve, $\eta^{(0)}_{s/d}$). The presence of SOC or ISB removes this degeneracy, making s-wave (red curve, η_s) the leading pairing instability and d-wave (blue curve, η_d) the subleading one. (b) The normalized SC gap along the X electron pocket as a function of the angle θ for different values of λ_2/λ_1.

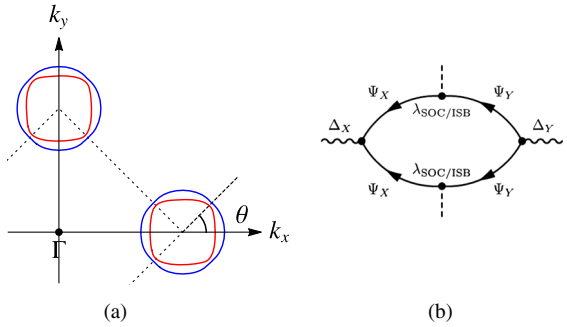

FIG. 3. (a) The Fermi surface in the presence of SOC or ISB consists of split inner (red) and outer (blue) electron pockets. (b) Feynman diagram representing the coupling between the gaps in the two electron pockets promoted by SOC or ISB. This coupling lifts the degeneracy between the s wave and d wave.

weight of the d_{xy} orbital on the X pocket is maximum. Recent ARPES experiments in FeSe suggest that λ_1 and λ_2 are comparable [52].

In terms of the averaged gaps Δ_X and Δ_Y, the s-wave and d-wave solutions correspond to $\Delta_s = \frac{1}{2}(\Delta_X + \Delta_Y)$ and $\Delta_d = \frac{1}{2}(\Delta_X - \Delta_Y)$. Using this notation, the degeneracy between s and d can be understood as a consequence of the fact that nematic fluctuations, peaked at $\boldsymbol{Q}_{\rm nem} = 0$, do not couple the gaps at the X and Y pockets, since they are displaced by the momentum $\mathbf{Q}_M = \mathbf{Q}_X + \mathbf{Q}_Y = (\pi, \pi)$. This suggests an enlarged $U(1) \times U(1)$ degeneracy of the SC ground state manifold, corresponding to two decoupled SC order parameters. To investigate the robustness of this enlarged degeneracy, we went beyond the linearized gap equations and computed the superconducting free energy to quartic order in the gaps (see the Supplemental Material [46]), obtaining

$$F_{\rm SC} = a(|\Delta_X|^2 + |\Delta_Y|^2) + \frac{u}{2}(|\Delta_X|^4 + |\Delta_Y|^4). \quad (5)$$

This form confirms that Δ_X and Δ_Y remain decoupled to higher orders in $F_{\rm SC}$. The consequences of this enlarged $U(1) \times U(1)$ degeneracy are severe: going beyond the mean-field approximation of Eq. (4), fluctuations of one SC channel suppress long-range order in the other channel, i.e., $T_{c,s} - T_{c,0} \propto -\langle \Delta_d^2 \rangle$. Such a pairing frustration is therefore detrimental to SC [53–56], suggesting that nematic fluctuations alone do not provide an optimal SC pairing mechanism in this system. Interestingly, previous investigations of SC induced by nematic fluctuations in different models also found nearly degenerate states [39,57].

Spin-orbit coupling (SOC) and inversion symmetry breaking (ISB).—The analysis above neglected a key property of the crystal structure of the FeSe plane: Because of the puckering of the Se atoms above and below the Fe square lattice, the actual crystallographic unit cell contains 2 Fe atoms. As a result, in the 2-Fe Brillouin zone (the folded BZ), the momentum $\boldsymbol{Q}_M = (\pi, \pi)$ becomes $\tilde{\mathbf{Q}} = 0$ (hereafter the tilde denotes a wave vector in the folded BZ). Thus, the two electron pockets become centered at the same momentum $\tilde{\mathbf{Q}} = (\pi, \pi)$ and overlap, as shown by the dashed lines in Fig. 1(a).

This property opens up the possibility of coupling the Δ_X and Δ_Y gaps and removing the enlarged $U(1) \times U(1)$ degeneracy. At the noninteracting level, this is accomplished by the atomic spin orbit coupling $\lambda_{\rm SOC} \boldsymbol{S} \cdot \boldsymbol{L}$, which couples the d_{xz} (d_{yz}) orbital associated with the $Y(X)$ pocket to the d_{xy} orbital associated with the $X(Y)$ pocket [48]:

$$\mathcal{H}_{\rm SOC} = \frac{i}{2}\lambda_{\rm SOC} \sum_{\boldsymbol{k}} \Psi_Y^\dagger (\tau_+ \otimes \sigma_1 + \tau_- \otimes \sigma_2) \Psi_X + \text{H.c.}, \quad (6)$$

where τ and σ are Pauli matrices in spinor and spin spaces, respectively. While in the normal state the SOC splits the two overlapping elliptical electron pockets centered at $\tilde{\mathbf{Q}} = (\pi, \pi)$ into inner and outer pockets [see Fig. 3(a) and the ARPES data of Ref. [41]], in the SC state it couples the gaps Δ_X and Δ_Y. For $\lambda_{\rm SOC}$ small compared to ϵ_m—the energy scale associated with the mismatch between the X and Y electron pockets—this coupling is given perturbatively by the Feynman diagram of Fig. 3(b), which gives the following contribution to the SC free-energy of Eq. (5):

$$\delta F_{\rm SC} = \gamma(\Delta_X \Delta_Y^* + \text{H.c.}). \quad (7)$$

As shown in the Supplemental Material [46], $\gamma \propto -\lambda^2$, implying that the SOC selects the s-wave state, with Δ_X and Δ_Y of the same sign, over the d-wave state, with Δ_X and Δ_Y of opposite signs. More importantly, it lifts the $U(1) \times U(1)$ degeneracy between the two pairing states, suppressing the negative interference of one pairing channel on the other. We confirmed this general conclusion by evaluating explicitly the gap equations in the A_{1g} (s-wave) and B_{2g} (d-wave) channels, finding that $\eta_s > \eta_d$ for all values of the nematic coupling constants, as shown in Fig. 2(a). Note that the SOC induces triplet components to these pairing states (see the Supplemental Material [46]).

Having established that the A_{1g} channel is the leading SC instability, we now discuss the angular dependence of the gaps $\Delta_{i/o}$ around the inner (i) and outer (o) electron pockets. When $\lambda_{\mathrm{SOC}} \ll \epsilon_m$, as it is apparent from Fig. 1(a), the outer electron pocket consists mostly of d_{xy} orbital spectral weight, whereas the inner pocket consists mostly of d_{xz}/d_{yz} spectral weight. The d_{xz} and d_{yz} gap functions have essentially the same angular dependence as in the case without SOC, shown previously in Fig. 2(b). Consequently, the gap anisotropy depends strongly on the ratio λ_1/λ_2 between the two nematic couplings. For $\lambda_1 \approx \lambda_2$, the gaps are nearly isotropic around the inner and outer pockets, whereas for $\lambda_1 < \lambda_2$ or $\lambda_1 > \lambda_2$, the gaps are anisotropic in both pockets.

The gap structure, however, changes dramatically in the case $\lambda_{\mathrm{SOC}} \gg \epsilon_m$ (with both still much smaller than the Fermi energy). In this case, the two reconstructed electron pockets are fully hybridized, implying that their orbital weights are similar. As a result, the SC gaps on the inner and outer pockets are weakly anisotropic for all values of the ratio λ_1/λ_2, whose main effect is to displace the position of the gap maxima. While for $\lambda_1 < \lambda_2$ the gap minima are located at the intersection points between the two unhybridized electron pockets, $\theta = \pm\pi/4$, for $\lambda_1 > \lambda_2$ the gap minima are found at the intersection points (see Fig. 4). Interestingly, recent ARPES experiments in monolayer FeSe observe gap maxima at $\theta = \pm\pi/4$ [58], whereas STM measurements in the intercalated $\mathrm{Li}_{1-x}(\mathrm{OH})_x\mathrm{FeSe}$ compound report gap minima at $\theta = \pm\pi/4$ [44].

Besides SOC, the inversion-symmetry breaking (ISB) at the interface of thin films also lifts the degeneracy between s wave and d wave in the case of FeSe thin films. In terms of the low-energy spinor states, ISB gives rise to the term [59]

$$H_{\mathrm{ISB}} = \lambda_{\mathrm{ISB}} \sum_{\boldsymbol{k}} \Psi_X^\dagger \frac{\tau_0 + \tau_3}{2} \Psi_Y + \mathrm{H.c.} \qquad (8)$$

Similarly to SOC, λ_{ISB} hybridizes the two electron pockets and favors s wave over d wave, lifting the degeneracy between the two states [Fig. 3(b)] and enhancing the s-wave pairing instability. As shown in the Supplemental Material [46], the effect of ISB on the angular dependence of the gap functions around the inner and outer pockets is very similar to the effect of SOC. The only difference is that because ISB barely couples to the d_{xy} orbitals, the gaps remain moderately anisotropic.

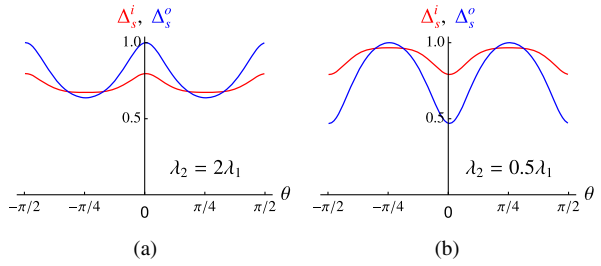

FIG. 4. Angular dependence of the SC gap along the inner (red) and outer (blue) electron pocket in the case where the SOC coupling is much larger than the electron pockets mismatch. The positions of the gap minima are controlled by λ_2/λ_1.

So far we considered only the zero-momentum contribution of the nematic fluctuations. In general, however, $\chi_{\mathrm{nem}}^{-1}(\mathbf{q}) = \xi_{\mathrm{nem}}^{-2} + q^2$. Thus, although small-momentum fluctuations do not couple the X and Y pockets, leaving the s-wave or d-wave degeneracy intact, large-momentum fluctuations couple them, giving rise to their own free-energy coupling γ' in Eq. (7). As shown in the Supplemental Material [46], however, $\gamma' \ll \gamma$, implying that the small-momentum approximation is sensible.

Besides SOC and ISB, other effects can lift the s-wave or d-wave degeneracy promoted by the dominant nematic fluctuations. For instance, magnetic fluctuations peaked at (π, π) would favor the d-wave state [60,61], whereas a momentum-independent electron-phonon interaction would favor the s-wave state. To the best of our knowledge, no sign of (π, π) magnetic order has been observed in FeSe thin films with only electron pockets. First-principle calculations for the momentum-independent phonon coupling estimate a resulting $T_c \lesssim 1$ K [62], an energy scale that may be too small to significantly lift the degeneracy, since $T_c \approx 40$ K in FeSe thin films.

Previous works have shown that forward-scattering phonons can lead to a sizable enhancement of T_c in FeSe films grown over $SrTiO_3$ or $BaTiO_3$ [18,20–24]. Indeed, the observation of a replica band in ARPES measurements highlights the importance of this phonon mode [16]. Similarly to the nematic fluctuations studied here, forward-scattering phonons are also peaked at zero momentum, and, therefore, are expected to also promote degenerate s-wave or d-wave SC states [24]. In this regard, the two pairing mechanisms may cooperate to promote a robust SC state, whose degeneracy is lifted by SOC or ISB. While a detailed analysis of this problem is beyond the scope of this work, it is tempting to attribute to this cooperative effect the fact that T_c is higher in FeSe films grown over titanium oxide interfaces as compared to other types of interfaces or other FeSe-based compounds.

Summary.—In summary, we showed that the combined effect of nematic fluctuations and SOC/ISB favors an s-wave state in electron-doped thin films of FeSe, in agreement with recent experimental proposals [42]. The role played by SOC and ISB is fundamental to lift the degeneracy with the subleading d-wave state, which suppresses the onset of long-range SC order. Although nematic fluctuations are momentum independent in our model, the gap function can acquire a pronounced angular dependence since the nematic order parameter couples differently to d_{xz}/d_{yz} and d_{xy} orbitals. Interestingly, in the regime where the SOC and ISB couplings are larger than the mismatch between the electron pockets, we obtain a gap function whose angular dependence agrees qualitatively with measurements in monolayer FeSe and intercalated $\mathrm{Li}_{1-x}(\mathrm{OH})_x\mathrm{FeSe}$. More generally, our work provides an

interesting framework in which superconductivity can develop in the presence of nematic fluctuations.

We thank A. Chubukov, S. Lederer, X. Liu, A. Millis, M. Khodas, S. Kivelson, S. Raghu, D. Scalapino, M. Schüt, Y. Wang, O. Vafek, and Y. Y. Zhao for fruitful discussions. This work was supported by the U.S. Department of Energy, Office of Science, Basic Energy Sciences, under Award No. DE-SC0012336.

*jkang@umn.edu

[1] I. I. Mazin, D. J. Singh, M. D. Johannes, and M. H. Du, Phys. Rev. Lett. **101**, 057003 (2008).
[2] P. J. Hirschfeld, M. M. Korshunov, and I. I. Mazin, Rep. Prog. Phys. **74**, 124508 (2011).
[3] D. N. Basov and A. V. Chubukov, Nat. Phys. **7**, 272 (2011).
[4] A. V. Chubukov, Annu. Rev. Condens. Matter Phys. **3**, 57 (2012).
[5] Q. Y. Wang *et al.*, Chin. Phys. Lett. **29**, 037402 (2012).
[6] D. F. Liu *et al.*, Nat. Commun. **3**, 931 (2012).
[7] S. L. He *et al.*, Nat. Mater. **12**, 605 (2013).
[8] S. Tan *et al.*, Nat. Mater. **12**, 634 (2013).
[9] W. H. Zhang *et al.*, Chin. Phys. Lett. **31**, 017401 (2014).
[10] J.-F. Ge, Z.-L. Liu, C. Liu, C.-L. Gao, D. Qian, Q.-K. Xue, Y. Liu, and J.-F. Jia, Nat. Mater. **14**, 285 (2014).
[11] P. Zhang *et al.*, Phys. Rev. B **94**, 104510 (2016).
[12] R. Peng *et al.*, Nat. Commun. **5**, 5044 (2014).
[13] B. Lei, J. H. Cui, Z. J. Xiang, C. Shang, N. Z. Wang, G. J. Ye, X. G. Luo, T. Wu, Z. Sun, and X. H. Chen, Phys. Rev. Lett. **116**, 077002 (2016).
[14] Y. Sun, W. Zhang, Y. Xing, F. Li, Y. Zhao, Z. Xia, L. Wang, X. Ma, Q.-K. Xue, and J. Wang, Sci. Rep. **4**, 6040 (2014).
[15] E. Pomjakushina, K. Conder, V. Pomjakushin, M. Bendele, and R. Khasanov, Phys. Rev. B **80**, 024517 (2009).
[16] J. J. Lee *et al.*, Nature (London) **515**, 245 (2014).
[17] F.-C. Hsu *et al.*, Proc. Natl Acad. Sci. U.S.A. **105**, 14262 (2008).
[18] Y.-Y. Xiang, F. Wang, D. Wang, Q.-H. Wang, and D.-H. Lee, Phys. Rev. B **86**, 134508 (2012).
[19] Y. C. Tian, W. H. Zhang, F. S. Li, Y. L. Wu, Q. Wu, F. Sun, G. Y. Zhou, L. Wang, X. Ma, Q.-K. Xue, and J. Zhao, Phys. Rev. Lett. **116**, 107001 (2016).
[20] L. Rademaker, Y. Wang, T. Berlijn, and S. Johnston, New J. Phys. **18**, 022001 (2016).
[21] Y. Zhou and A. J. Millis, Phys. Rev. B **93**, 224506 (2016).
[22] Z.-X. Li, F. Wang, H. Yao, and D. H. Lee, Science bulletin **61**, 925 (2016).
[23] Y. Wang, K. Nakatsukasa, L. Rademaker, T. Berlijn, and S. Johnston, Supercond. Sci. Technol. **29**, 054009 (2016).
[24] M. L. Kulic and O. V. Dolgov, arXiv:1607.00843.
[25] J. Shiogai, Y. Ito, T. Mitsuhashi, T. Nojima, and A. Tsukazaki, Nat. Phys. **12**, 42 (2016).
[26] Z. R. Ye *et al.*, arXiv:1512.02526.
[27] Y. Miyata, K. Nakayama, K. Sugawara, T. Sato, and T. Takahashi, Nat. Mater. **14**, 775 (2015).
[28] X. H. Niu *et al.*, Phys. Rev. B **92**, 060504 (2015).
[29] L. Zhao *et al.*, Nat. Commun. **7**, 10608 (2016).
[30] M. D. Watson *et al.*, Phys. Rev. B **91**, 155106 (2015).
[31] A. V. Chubukov, R. M. Fernandes, and J. Schmalian, Phys. Rev. B **91**, 201105 (2015).
[32] A. V. Chubukov, M. Khodas, and R. M. Fernandes, arXiv: 1602.05503.
[33] F. Wang, S. A. Kivelson, and D.-H. Lee, Nat. Phys. **11**, 959 (2015).
[34] R. Yu and Q. Si, Phys. Rev. Lett. **115**, 116401 (2015).
[35] J. K. Glasbrenner, I. I. Mazin, H. O. Jeschke, P. J. Hirschfeld, R. M. Fernandes, and R. Valenti, Nat. Phys. **11**, 953 (2015).
[36] Y. Zhang *et al.*, Phys. Rev. B **94**, 115153 (2016).
[37] C. H. P. Wen *et al.*, Nat. Commun. **7**, 10840 (2016).
[38] D. Huang, T. A. Webb, S. Fang, C.-L. Song, C.-Z. Chang, J. S. Moodera, E. Kaxiras, and J. E. Hoffman, Phys. Rev. B **93**, 125129 (2016).
[39] H. Yamase and R. Zeyher, Phys. Rev. B **88**, 180502(R) (2013).
[40] P. T. Dumitrescu, M. Serbyn, R. T. Scalettar, and A. Vishwanath, Phys. Rev. B **94**, 155127 (2016).
[41] S. V. Borisenko *et al.*, Nat. Phys. **12**, 311 (2016).
[42] Q. Fan *et al.*, Nat. Phys. **11**, 946 (2015).
[43] R. Peng *et al.*, Phys. Rev. Lett. **112**, 107001 (2014).
[44] Z. Du, X. Yang, H. Lin, D. Fang, G. Du, J. Xing, H. Yang, X. Zhu, and H.-H. Wen, Nat. Commun. **7**, 10565 (2016).
[45] V. Cvetkovic and O. Vafek, Phys. Rev. B **88**, 134510 (2013).
[46] See Supplemental Material at http://link.aps.org/supplemental/10.1103/PhysRevLett.117.217003 for the classification of various pairings and detailed information of the gap structure, which includes Refs. [41,45,47].
[47] J. Kang, A. F. Kemper, and R. M. Fernandes, Phys. Rev. Lett. **113**, 217001 (2014).
[48] R. M. Fernandes and O. Vafek, Phys. Rev. B **90**, 214514 (2014).
[49] Y. Schattner, S. Lederer, S. A. Kivelson, and E. Berg, Phys. Rev. X **6**, 031028 (2016).
[50] Z-X. Li, F. Wang, H. Yao, and D. H. Lee, arXiv:1512.04541.
[51] To be consistent with previous works, the irreducible representations refer to the actual crystallographic 2-Fe Brillouin zone coordinate system (K_x, K_y), i.e., B_{2g} transforms as $k_x^2 - k_y^2$ (or $K_x K_Y$) and B_{1g} transforms as $k_x k_y$ (or $K_x^2 - K_y^2$).
[52] A. Fedorov *et al.*, arXiv:1606.03022.
[53] R. M. Fernandes and A. J. Millis, Phys. Rev. Lett. **110**, 117004 (2013).
[54] F. Yang, F. Wang, and D.-H. Lee, Phys. Rev. B **88**, 100504 (2013).
[55] P. M. R. Brydon, S. Das Sarma, H.-Y. Hui, and J. D. Sau, Phys. Rev. B **90**, 184512 (2014).
[56] Y. Wang, G. Y. Cho, T. L. Hughes, and E. Fradkin, Phys. Rev. B **93**, 134512 (2016).
[57] S. Lederer, Y. Schattner, E. Berg, and S. A. Kivelson, Phys. Rev. Lett. **114**, 097001 (2015).
[58] Y. Zhang, J. J. Lee, R. G. Moore, W. Li, M. Yi, M. Hashimoto, D. H. Lu, T. P. Devereaux, D.-H. Lee, and Z.-X. Shen, Phys. Rev. Lett. **117**, 117001 (2016).
[59] N. Hao and J. Hu, Phys. Rev. X **4**, 031053 (2014).
[60] M. Khodas and A. V. Chubukov, Phys. Rev. Lett. **108**, 247003 (2012).
[61] A. Hinojosa and A. V. Chubukov, Phys. Rev. B **91**, 224502 (2015).
[62] B. Li, Z. W. Xing, G. Q. Huang, and D. Y. Xing, J. Appl. Phys. **115**, 193907 (2014).